Catalysis Science & Technology

Catalytic Direct Oxidation of Methane to Methanol by Redox of Copper Mordenite

Journal:	*Catalysis Science & Technology*
Manuscript ID	CY-ART-01-2021-000125.R1
Article Type:	Paper
Date Submitted by the Author:	25-Feb-2021

Complete List of Authors:	Ohyama, Junya; Kumamoto University, Faculty of Advanced Science and Technology Hirayama, Airi; Kumamoto University, Graduate School of Science and Technology Tsuchimura, Yuka; Kumamoto University, Graduate School of Science and Technology Kondou, Nahoko; Kumamoto University, Faculty of Advanced Science and Technology Yoshida, Hiroshi; Kumamoto Daigaku, Machida, Masato; Kumamoto University, Applied Chemistry and Biochemistry Nishimura, Shun; Japan Advanced Institute of Science and Technology, Graduate School of Advanced Science and Technology Kato, Kazuo; Japan Synchrotron Radiation Research Institute, Miyazato, Itsuki; Hokkaido University Takahashi, Keisuke; Hokkaido University, Department of Chemistry; National Institute for Materials Science, Center for Materials research by Information

SCHOLARONE™
Manuscripts

ARTICLE

Catalytic Direct Oxidation of Methane to Methanol by Redox of Copper Mordenite

Received 00th January 20xx,
Accepted 00th January 20xx

DOI: 10.1039/x0xx00000x

Junya Ohyama,*[a] Airi Hirayama,[b] Yuka Tsuchimura,[b] Nahoko Kondou,[a] Hiroshi Yoshida,[a] Masato Machida,[a] Shun Nishimura,[c] Kazuo Kato,[d] Itsuki Miyazato[e] and Keisuke Takahashi[e]

Expectations for industrial implementation of direct conversion of CH_4 to CH_3OH are growing with the increasing demand for energy-efficient chemical processes. In this study, catalytic production of CH_3OH by direct oxidation of CH_4 with O_2 was performed using Cu zeolite catalysts in a $CH_4/O_2/H_2O$ flow reaction. Among the various Cu zeolites investigated, the Cu-MOR catalyst exhibited relatively high CH_3OH production with a turnover number of 7.4 mol_{CH3OH}/mol_{Cu} over 24 h (CH_4 conversion: 0.011%). The catalytically active Cu species and catalytic cycle were investigated by in-situ simultaneous X-ray absorption and infrared spectroscopy. The results suggest that the key to the catalytic cycle over Cu-MOR is the redox of Cu(I)/Cu(II) species. Furthermore, H_2O-adsorption-included dynamic Cu species are revealed to be catalytically active.

Introduction

Direct oxidation of CH_4 to CH_3OH is a challenging reaction that is being carefully investigated by developing various catalysts, including enzymes, complexes and inorganic solid materials, for its implementation in industrial applications. The ultimate aim is to realize an energy-efficient chemical process to produce CH_3OH.[1-5] In the current industrial chemical process, CH_4 is indirectly converted to CH_3OH via reformation and hydrogenation reactions, which require high temperature and pressure.[2, 6] CH_4 is also increasingly used as a clean fuel for vehicles and power generation; however, decreasing the temperature for removal of unburned CH_4, which has a high greenhouse gas effect, is challenging because of the very stable nature of CH_4.[7, 8] In nature, methane monooxygenase converts CH_4 to CH_3OH at ambient temperature and pressure using Cu and Fe active sites in its particulate and soluble forms, respectively.[9] For industrial applications of the CH_4-to-CH_3OH reaction, heterogeneous catalysts made of inorganic solid materials are preferable to enzyme and complex catalysts because the former offer much higher durability under the reaction conditions than the latter.[10] Consequently, solid catalysts with bioinspired active sites, particularly Cu and Fe zeolites, have been explored.[4, 10-12] Gas flow reaction systems have been tested for CH_4-to-CH_3OH conversion using Cu and Fe zeolites. Continuous CH_3OH production has been demonstrated using a Cu zeolite in a $CH_4/O_2/H_2O$ flow; however, the CH_3OH production rate has been still very low.[13, 14]

Heterogeneous catalytic reaction systems for direct synthesis of CH_3OH from CH_4 using NOx as an oxidant have also been designed that show promising production rates, but CH_3OH selectivity is decreased by overoxidation.[15, 16] Using H_2O_2 as an oxidant can increase CH_3OH production with high selectivity; however, this approach is more expensive than CH_3OH production by the conventional method.[17-20] Because the catalytic CH_3OH production has been still far from practical use, a chemical looping process in which CH_4 is transformed stepwise to CH_3OH on metal (usually Cu) zeolites has attracted attention.[6, 12, 21-24] This process is not catalytic but is composed of stoichiometric reaction steps: Cu zeolites are activated by heat treatment under O_2, reacted with CH_4 to form methoxy-adsorbed Cu zeolites and finally water vapour is flowed into the system to extract CH_3OH and leave deactivated Cu zeolites. The chemical looping process allows selective CH_3OH formation with higher productivity than continuous CH_3OH production by the $CH_4/O_2/H_2O$ flow reaction; however, the production rate still does not meet the level needed for industrial use.[6]

In this study, the continuous catalytic production of CH_3OH by $CH_4/O_2/H_2O$ flow reaction is focused on. Various Cu zeolites are tested for $CH_4/O_2/H_2O$ flow reaction under different reaction conditions from the previous studies.[13, 14] As a result, a catalytic reaction system showing CH_3OH and HCHO production with turnover numbers (TONs) of 7.4 mol_{CH3OH}/mol_{Cu} and 10.9 $mol_{CH3OH+HCHO}/mol_{Cu}$ in 24 h is demonstrated using a Cu-MOR catalyst. The catalytic cycle and its important step are determined by in-situ observation of Cu zeolites by simultaneous XAFS and DRIFT spectroscopies.

[a] Faculty of Advanced Science and Technology, Kumamoto University
2-39-1 Kurokami, Chuo-ku, Kumamoto, 860-8555, Japan.
[b] Department of Applied Chemistry and Biochemistry, Graduate School of Science and Technology, Kumamoto University
2-39-1 Kurokami, Chuo-ku, Kumamoto, 860-8555, Japan.
[c] Graduate School of Advanced Science and Technology, Japan Advanced Institute of Science and Technology (JAIST)
1-1 Asahidai, Nomi, 923-1292, Japan.
[d] Japan Synchrotron Radiation Research Institute
1-1 Kouto, Sayo-cho, Sayo-gun Hyogo, 679-5198, Japan
[e] Department of Chemistry, Hokkaido University
N-15 W-8, Sapporo, 060-0815, Japan

† Electronic Supplementary Information (ESI) available: In-situ XANES and FT EXAFS spectra; gas flow schemes; schematic diagram of the optical system used for the in-situ XAFS and DRIFT spectral measurements. See DOI: 10.1039/x0xx00000x

Results and Discussion

Catalytic reaction

Several Cu zeolites were prepared by an ion exchange method using $Cu(CH_3COO)_2 \cdot H_2O$ and proton-exchanged MOR, FAU, BEA and MFI zeolites. The Cu zeolites are referred to as Cux-TYPy where x, TYP, and y mean Cu loading (wt%), framework type and Si/Al ratio, respectively. Figure 1 shows the product amounts of $CH_4/O_2/H_2O$ flow reaction for 24 h over the various Cu zeolites at 300 °C. The time course of CH_3OH and carbon dioxide (CO_2) production is shown in Figure S1(a) and (b). CH_3OH was produced over all the Cu zeolites for 24 h. CO_2 was also detected, although carbon monoxide (CO) was not detected. Formaldehyde (HCHO) was observed in the trapped liquid containing the reaction products as presented in Figure 1 and Table 1. In contrast, no significant production of formic acid (<0.03 mmol g_{cat}^{-1}) was detected for all catalysts. The highest CH_3OH production was obtained over Cu2.0-MOR10, where CH_3OH was continuously produced at least for 24 h and the integrated CH_3OH amount after 24 h was estimated to be 2.3 $mmol_{CH3OH}\ g_{cat}^{-1}$ for 24 h with an average rate of 1.6 $\mu mol_{CH3OH}\ min^{-1}\ g_{cat}^{-1}$ at CH_4 conversion of 0.011%. As a control, H-MOR10 before Cu exchange was used in the $CH_4/O_2/H_2O$ reaction. In this case, little CH_3OH (<0.1 $\mu mol_{CH3OH}\ min^{-1}\ g_{cat}^{-1}$) and no other products were observed (Figure 1(g) and S1). Therefore, Cu is the active species in CH_3OH production. The TON over 24 h for Cu2.0-MOR10 calculated in mol_{CH3OH}/mol_{Cu} was 7.4. This indicates that Cu2.0-MOR10 acts as a catalyst for partial oxidation of CH_4 to CH_3OH. In addition, the TON in terms of CH_3OH and HCHO was 10.9 $mol_{CH3OH+HCHO}/mol_{Cu}$ over 24 h. The other Cu zeolites also showed continuous CH_3OH and HCHO production, although their activity was lower than that of Cu2.0-MOR10. The TONs of the Cu zeolites are summarised in Table 1. The two Cu-MOR catalysts showed higher TONs than those of the other zeolites with different frameworks. It is considered that the Cu-MOR catalysts have highly active sites for the $CH_4/O_2/H_2O$ reaction. The CH_3OH production rate (1.6 $\mu mol_{CH3OH}\ min^{-1}\ g_{cat}^{-1}$) is largely improved in comparison with that obtained in previous studies of $CH_4/O_2/H_2O$ reaction over Cu-MOR.[13] The keys to the improved CH_3OH production would be the higher O_2 partial pressure and/or higher reaction temperature by 25-50 °C than were used in previous studies, as seen later. It should also be noted that the CO_2 production of Cu-MOR (Figure 1 and Table 1) was also higher than those reported previously.[13] Thus, the improved CH_3OH production accompanies complete oxidation of CH_4 to CO_2 production, of which reduction will be an issue to be tackled in the future study.

CH_4 oxidation was carried out without H_2O(g) or O_2 using Cu2.0-MOR10 (Figure 1(h), (i), S1(c) and Table 1 entry 7-8). Without H_2O(g) (denoted as CH_4/O_2), CH_4 was oxidized to produce CH_3OH; however, the amount of CH_3OH (0.3 mmol g_{cat}^{-1} for 24 h) was 1/7 of that produced under the $CH_4/O_2/H_2O$ flow (Figure 1(h) and S1(c)). In addition, both CO and CO_2 formed more than those under the $CH_4/O_2/H_2O$ flow. These results indicate that O_2 works as an oxidant and H_2O(g) effectively increases the selectivity to CH_3OH. In the absence of O_2 (denoted as CH_4/H_2O), CH_3OH was produced selectively without significant detections of CO and CO_2. The amount of CH_3OH produced (0.03 $mmol_{CH3OH}\ g_{cat}^{-1}$ for 24 h, 1.21 $\mu mol_{MeOH}\ g_{cat}^{-1}\ h^{-1}$) was in the same order of magnitude as that on Cu-CHA reported previously (5.30 $\mu mol_{MeOH}\ g_{cat}^{-1}\ h^{-1}$),[25] although it was much less than that obtained under the $CH_4/O_2/H_2O$ flow. This result indicates that H_2O can also behave as an oxidant for selective oxidation of CH_4;[25] however, the oxidation ability of H_2O is lower than that of O_2. Therefore, O_2 and H_2O act as relatively strong and weak oxidants, respectively, for CH_4 oxidation over Cu2.0-MOR10. In addition, H_2O(g) suppressed overoxidation of CH_4 to CO and/or CO_2.

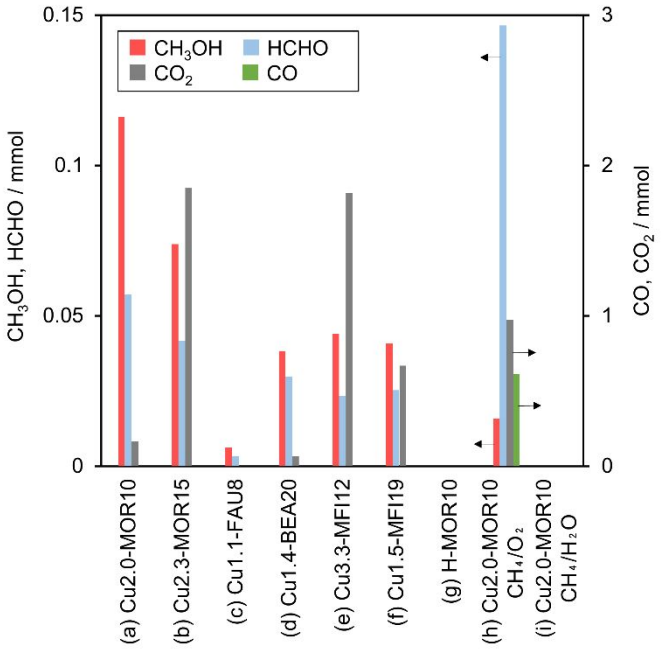

Figure 1. Product amounts of $CH_4/O_2/H_2O$ rection for 24 h over (a) Cu2.0-MOR10, (b) Cu2.3-MOR15, (c) Cu1.4-BEA20, (d) Cu1.1-FAU8, (e) Cu3.3-MFI12, (f) Cu1.5-MFI19 and (g) H-MOR10, together with those of (h) CH_4/O_2 and (i) CH_4/H_2O reaction for 24 h over Cu2.0-MOR10. $CH_4/O_2/H_2O$ reaction conditions: catalyst 50 mg, 300 °C, CH_4 (48 mL min^{-1}) + O_2 (2 mL min^{-1}) + N_2 (50 mL min^{-1}) + water vapour (H_2O(g); 0.5 g h^{-1}). CH_4/O_2 reaction conditions: catalyst 50 mg, 300 °C, CH_4 (48 mL min^{-1}) + O_2 (2 mL min^{-1}) + N_2 (60 mL min^{-1}). CH_4/H_2O reaction conditions: catalyst 50 mg, 300 °C, CH_4 (48 mL min^{-1}) + N_2 (52 mL min^{-1}) + H_2O(g) (0.5 g h^{-1}).

This journal is © The Royal Society of Chemistry 20xx

Please do not adjust margins

ARTICLE

Table 1. CH_3OH yield, production rate, TON, partial oxidation selectivity and CH_4 conversion of $CH_4/O_2/H_2O$ reaction for 24 h over Cu zeolites (entry 1-6) together with those of CH_4/O_2 and CH_4/H_2O reaction over Cu2.0-MOR10 (entry 7-8).

Entry	Cu-zeolite	CH_3OH yield [a] ($mmol\ g_{cat}^{-1}$)	CH_3OH production rate [b] ($\mu mol_{CH3OH}\ g_{cat}^{-1} min^{-1}$)	HCHO yield [c] ($mmol\ g_{cat}^{-1}$)	CO_2 [d] ($mmol\ g_{cat}^{-1}$)	CO [d] ($mmol\ g_{cat}^{-1}$)	TON for CH_3OH (mol_{CH3OH}/mol_{Cu})	TON for CH_3OH + HCHO ($mol_{CH3OH+HCHO}/mol_{Cu}$)	CH_3OH + HCHO selectivity [e] (%)	CH_4 conversion (%)
1	Cu2.0-MOR10	2.3	1.6	1.1	3.2	0.0	7.4	10.9	52	0.011
2	Cu2.3-MOR15	1.4	1.0	0.8	36.4	0.0	4.0	6.2	6	0.064
3	Cu1.1-FAU8	0.1	0.1	0.1	0.0	0.0	0.7	1.0	100	0.000
4	Cu1.4-BEA20	0.7	0.5	0.6	1.3	0.0	3.2	5.9	50	0.004
5	Cu3.3-MFI12	0.9	0.6	0.5	35.7	0.0	1.7	2.6	4	0.061
6	Cu1.5-MFI19	0.8	0.6	0.5	13.1	0.0	3.3	5.4	9	0.024
7 [f]	Cu2.0-MOR10	0.3	0.2	2.9	19.4	12.2	0.6	9.9	10	0.057
8 [g]	Cu2.0-MOR10	0.03	0.0	0.0	0.0	0.0	0.0	0.0	100	0.000

[a] Average amount of GC-FID and HPLC analysis. The errors of quantitative analysis by GC-FID and HPLC (error = GC or HPLC - Average) were within 0.1 mmol g_{cat}^{-1}. [b] Averaged over 24 h. [c] Evaluated by HPLC. [d] Evaluated by GD-TCD. [e] Calculated by (CH_3OH + HCHO) / (CH_3OH + HCHO + CO_2 + CO). [f] Results of CH_4/O_2 reaction. CH_3OH amount was evaluated by HPLC. [g] Results of CH_4/H_2O reaction. CH_3OH amount was evaluated by GC-FID.

Redox of Cu zeolites

In-situ XAFS and DRIFT spectral measurements were performed to investigate Cu2.0-MOR10 during the $CH_4/O_2/H_2O$ reaction. The variation of conditions during the in-situ XAFS and DRIFTS measurements are shown in Scheme 1. After O_2 pretreatment, the following gasses were flowed through the in-situ cell containing Cu zeolite at 300 °C: (1) $CH_4/O_2/H_2O$, i.e., the reaction gas; (2) O_2/H_2O, i.e., oxidative gas; (3) CH_4/H_2O, i.e., reductive gas. Meanwhile, Cu K-edge XAFS and DRIFT spectra were simultaneously measured. Each type of gas flow conditions (1) to (3) was continued until the induced spectral change was completed. Figure 2 shows the Cu K-edge X-ray absorption near-edge structure (XANES) spectra of Cu2.0-MOR10 before and after O_2 pretreatment and after exposure to flow conditions (1) to (3). All spectra during Scheme 1 are presented in Figure S2. The XANES spectra before and after O_2 pretreatment exhibit the features of hydrated and dehydrated Cu(II) species, respectively.[26] In particular, the dehydrated Cu(II) species formed after O_2 pretreatment shows a shoulder peak at 8988 eV consistent with the 1s to 4p electronic transition of the square planar structure of dehydrated Cu(II).[26-28] Under the $CH_4/O_2/H_2O$ flow, the spectral features somewhat returned to those of hydrated Cu(II), as represented by the decrease in the intensity of the shoulder at 8988 eV. The O_2/H_2O flow decreased the intensity of the shoulder peak at 8984 eV, whereas the CH_4/H_2O flow increased it. The shoulder peak at 8984 eV is assigned to the 1s to 4p electronic transition of Cu(I) species.[26, 29] Thus, the change of the peak at 8984 eV demonstrates the redox reactions of Cu species in Cu2.0-MOR10 under the reaction conditions. It should be noted that the spectrum under the $CH_4/O_2/H_2O$ reaction gas flow conditions is intermediate between those under the oxidative and reductive gas flows. Therefore, Cu2.0-MOR10 in the $CH_4/O_2/H_2O$ reaction is in the middle of the redox cycle between Cu(II) and Cu(I).

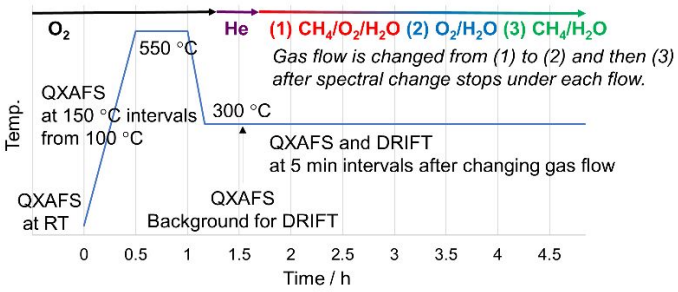

Scheme 1. Variations of temperature and gas flow during the in-situ XAFS and DRIFT spectral measurements. Gas flow conditions: (1) CH_4 (48 mL min^{-1})/O_2 (2 mL min^{-1})/H_2O(g) (0.5 g h^{-1})/He (50 mL min^{-1}); (2) O_2 (2 mL min^{-1})/H_2O(g) (0.5 g h^{-1})/He (50 mL min^{-1}); (3) CH_4 (48 mL min^{-1})/H_2O(g) (0.5 g h^{-1}) /He (50 mL min^{-1}).

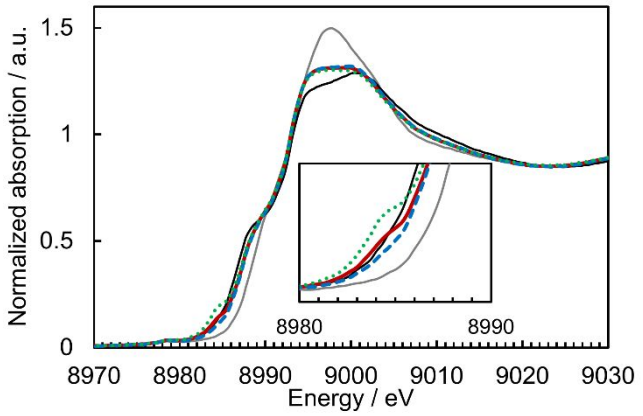

Figure 2. In-situ Cu K-edge XANES spectra of Cu2.0-MOR10 obtained according to Scheme 1. XANES spectra before (grey line) and after O_2 pretreatment (black line) and those after exposure to (1) $CH_4/O_2/H_2O$ (reaction gas, red line), (2) O_2/H_2O (oxidative gas, blue dashed line) and (3) CH_4/H_2O (reductive gas, green dotted line). Inserted graph: the enlarged view of pre-edge peak region at 8980-8990 eV.

The difference XANES spectra of (1) $CH_4/O_2/H_2O$ and (3) CH_4/H_2O from one after (2) O_2/H_2O were obtained as displayed in Figure 3(a) to extract the spectral variation of active Cu species from oxidized form to reduced one. Both difference spectra show the same feature, indicating that an identical reduced Cu species is formed by the gas flows (1) and (3), and the amount of reduce Cu species after the reductive gas flow (3) is larger than that after the reaction gas flow (1). In order to investigate the Cu species showing the redox, XANES spectra of oxidized and reduced form of Cu species are simulated by a finite-difference method for near-edge structure (FDMNES) as presented in Figure 3(b).[30] The μ-1,2-peroxo di-Cu(II) species ((i) in Figure 3(b)) and the bis(μ-oxo) di-Cu(II) species ((ii) in Figure 3(b)) are assumed as the possible active structures, and the linearly coordinated Cu(I) species ((iii) in Figure 3(b)) as the reduced form.[31, 32] Although trinuclear Cu(II) species and other Cu(II) oxo clusters can also be active oxidized forms of Cu species,[33] they are considered difficult to be formed compared to dinuclear Cu(II) species assuming such clusters are formed by diffusion and encountering of hydrated Cu species as described later. Thus, the spectral variation from the dinuclear Cu(II) species to the Cu(I) species was calculated as presented in Figure 3(c). The difference spectrum between the μ-1,2-peroxo di-Cu(II) species and the Cu(I) species ((iii)-(i) in Figure 3(c)) well captures the spectral feature of the experimental data (Figure 3(a)) in comparison with the difference spectrum between the bis(μ-oxo) di-Cu(II) species and the Cu(I) species ((iii)-(ii) in Figure 3(c)). As another possibility of the reduced form observed, the CH_3 adsorbed μ-1,2-peroxo di-Cu species, namely, partially reduced Cu(II) species ((iv) in Figure 3(b)), was also assumed; however, the difference spectrum between the μ-1,2-peroxo di-Cu(II) species with and without CH_3 ((iv)-(i) Figure 3(c)) is different from the experimental data feature. Thus, the μ-1,2-peroxo di-Cu(II) species and the Cu(I) species in the figure are proposed as oxidized and reduced forms of redox active Cu species in MOR. It should be noted that the simulation results do not deny formation of μ-oxo di-Cu species as active species because active species cannot stably exist during the reaction. It should also be noted that the experimental spectra show much smaller pre-edge peak intensity due to Cu(I) species than the simulated one even after the reductive gas flow (3). Based on estimation from the pre-edge peak intensity due to the Cu(I) species, about 20 % of Cu species in Cu2.0-MOR10 is involved in the redox cycle. Therefore, a part of Cu species in Cu2.0-MOR10 is considered catalytically active for the CH_4 oxidation by the redox cycle via the Cu(I) species and the μ-1,2-peroxo di-Cu(II) species.

Cu2.0-MOR10 was further investigated by Cu K-edge XAFS measurements under the following control conditions (Scheme S1): the O_2-pretreated Cu2.0-MOR10 was reduced by dry CH_4 flow and then treated with wet He flow (Figure S3). The XANES spectra obtained after the dry CH_4 and wet He treatments are shown in Figure S4. The intensity of the peak at 8984 eV related to Cu(I) decreased after the wet treatment, consistent with a previous study.[1] Under the reaction gas flow containing O_2, the peak intensity at 8984 eV diminished (Figure S4), indicating that the remaining Cu(I) under wet conditions was oxidized to Cu(II) by O_2. This suggests that O_2 is the stronger oxidant than H_2O in the Cu redox cycle under $CH_4/O_2/H_2O$ reaction gas flow.

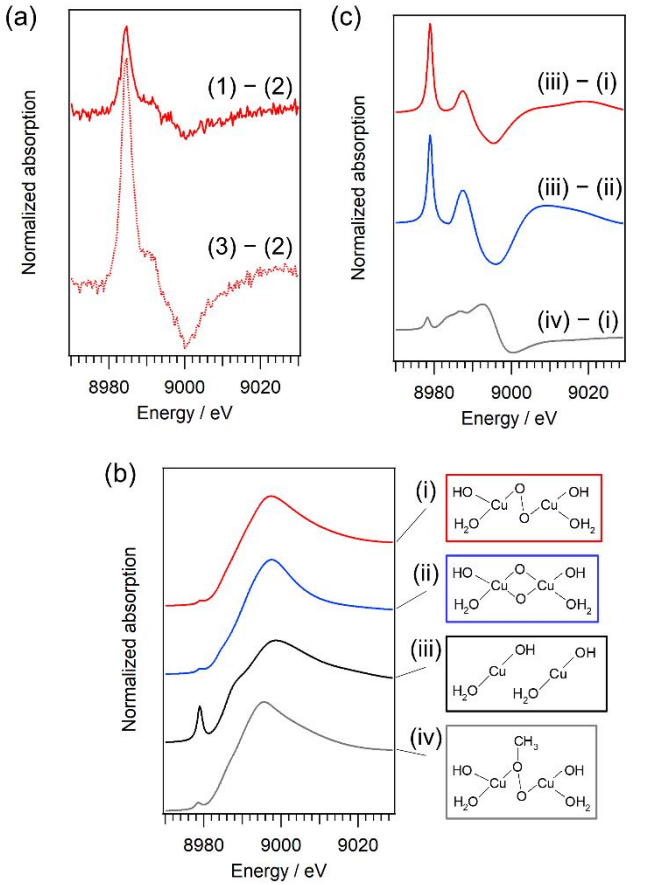

Figure 3. (a) Difference XANES spectra of (1) $CH_4/O_2/H_2O$ (red solid) and (3) CH_4/H_2O (red dotted) from one after (2) O_2/H_2O. (b) Simulated XANES spectra of the μ-1,2-peroxo di-Cu(II) species (red), the bis(μ-oxo) di-Cu(II) species (blue), the linearly coordinated Cu(I) species (black) and the μ-1,2-peroxo di-Cu(II) species with CH_3 (gray). (c) Difference simulated XANES spectra of the Cu(I) species from andμ-1,2-peroxo di-Cu(II) (red) and the bis(μ-oxo) di-Cu(II) (blue); the one of μ-1,2-peroxo di-Cu(II) with CH_3 from the μ-1,2-peroxo di-Cu(II) (gray).

This journal is © The Royal Society of Chemistry 20xx

Please do not adjust margins

Figure 4(a) presents the variation of the absorbance at 8984 eV in the Cu K-edge XANES spectra of Cu2.0-MOR10 under flow conditions (1) to (3). As described above, the absorbance at 8984 eV caused by Cu(I) increased under $CH_4/O_2/H_2O$ (1), decreased under O_2/H_2O (2), and then increased under CH_4/H_2O (3). For comparison, Cu1.1-FAU8, which has much lower activity than that of Cu2.0-MOR10, was investigated in the same manner as for Cu2.0-MOR10. The XANES spectra of Cu1.1-FAU8 before and after O_2 pretreatment and after exposure to flow conditions (1) to (3) are shown in Figure S5 and the change in absorbance at 8984 eV is presented in Figure 4(b). O_2 pretreatment of Cu1.1-FAU8 formed dehydrated Cu(II), and exposure of Cu1.1-FAU8 to $CH_4/O_2/H_2O$ (1) generated Cu(I) species, as indicated by the appearance and increase in the intensity of a peak at 8984 eV, whereas the spectral change caused by the hydration of Cu(II), e.g., a decrease of the absorbance at 8984 eV, was hardly observed. Thus, Cu2.0-MOR10 showed a larger spectral change induced by the reaction gas (1) (Figure 2) than was the case for Cu1.1-FAU8. One can consider that Cu2.0-MOR10 has more flexible/mobile Cu species than Cu1.1-FAU8. In the case of Cu1.1-FAU8, the XANES spectrum did not change even when the gas flow was switched to the oxidative gas (2), indicating that the Cu(I) species was not oxidized to Cu(II) by the oxidative gas flow. However, the reductive gas (3) increased the peak intensity at 8984 eV related to Cu(I) species. Thus, Cu1.1-FAU8 can be reduced but not oxidized under the investigated reaction conditions. The hardly oxidized Cu(I) species is thus the reason for the low catalytic activity of Cu1.1-FAU8. The reversible redox reaction of Cu2.0-MOR10 between Cu(II) and Cu(I), in particular, the oxidation of Cu(I) to Cu(II), is the key feature of its catalytic behaviour in the $CH_4/O_2/H_2O$ reaction.

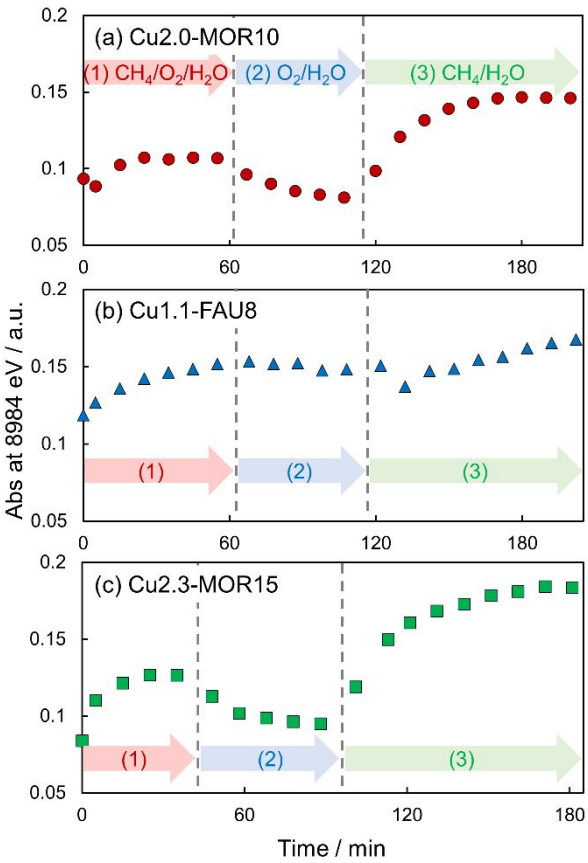

Figure 4. Redox behaviour of Cu zeolites: variation of absorbance at 8984 eV in the Cu K-edge XANES spectra of (a) Cu2.0-MOR10 (red circles), (b) Cu1.1-FAU8 (blue triangles) and (c) Cu2.3-MOR15 (green squares) under the flow conditions (1) to (3).

The redox behaviour of the other Cu-MOR catalyst, Cu2.3-MOR15, was also investigated. Similar to Cu2.0-MOR10, Cu2.3-MOR15 showed spectral changes consistent with the redox reaction between Cu(II) and Cu(I) with the variation of the gas flow conditions (Figure S6). These results strongly support that the oxidation step of Cu(I) to Cu(II) is important for the $CH_4/O_2/H_2O$ reaction. To further investigate the redox properties of the Cu-MOR catalysts, the time courses of the peak absorbance caused by Cu(I) for the two Cu-MOR catalysts were compared (Figure 4). The initial absorbance of the two samples was the same; however, the absorbance of Cu2.0MOR10 with high catalytic activity was lower than that of Cu2.3-MOR15 after exposure to $CH_4/O_2/H_2O$ (1). These results suggest that Cu2.0-MOR10 is more easily oxidized than Cu2.3-MOR15 in the reaction conditions. Evaluation of the reduction rate of the catalysts by CH_4 from the initial rate of change in the peak absorbance upon switching the gas flow from (2) to (3) revealed that Cu2.3-MOR15 showed faster reduction of Cu(II) than that of Cu2.0-MOR10. This result suggests that the fast reduction of Cu(II) by CH_4 does not directly contribute to improvement of partial oxidation of CH_4 (Figure 1 and Table 1). Rather, the fast reduction of Cu(II) causes the high CO_2 production (Figure 1 and Table 1). Thus, the oxidation of Cu(I) by O_2 or its relative rate to the reduction of Cu(II) are considered important for the catalytic partial oxidation of CH_4. Accordingly, the improved catalytic CH_3OH production (Figure 1(a)) can be

explained by Cu ion oxidation being promoted by the higher O_2 partial pressure used here than that in the previous study using Cu-MOR.[13]

Dynamic structure

The structures of Cu zeolites were investigated by Cu K-edge extended XAFS (EXAFS) spectral analysis (Figure S7–S11). Figure 5(a) shows the Fourier-transformed (FT) k^2-weighted EXAFS spectra of Cu2.0-MOR10 after O_2 pretreatment and exposure to flow conditions (1) to (3). All spectra show peaks at around 1.5 Å and 2-3 Å. The structural parameters obtained by the curve fitting analysis is presented in Table S1. The first shell at 1.5 Å is assigned to Cu-O scattering, and the second shell is composed of Cu-Al and Cu-Cu scatterings with ca. 2.7 and 3.0 Å of bond distances, respectively. The assignment is consistent with the previous report.[34] After the O_2 pretreatment, the coordination number of Cu-Al (CN(Cu-Al)) is larger than CN(Cu-Cu). Then, exposure to $CH_4/O_2/H_2O$ (1) decreased the CN(Cu-Al) and instead increased the CN(Cu-Cu) as the peak intensity at 2.2 Å decreased and the peak appeared at 2.6 Å. The spectral variation suggests that Cu species coordinated by the MOR framework are formed by O_2 pretreatment, and are moved to form Cu-Cu bond, in other words, multimeric Cu(II) species such as the μ-1,2-peroxo di-Cu(II) in the reaction gas flow (1).[31-33] Although the structural parameters were not significantly changed by the oxidative and reductive gas flow conditions, (2) and (3), respectively, slight variation of peak intensities at 1.5, 2.2 and 2.6 Å were observed in Figure 5(a) probably due to the redox reactions Cu species. For comparison, the FT-EXAFS spectra of Cu1.1-FAU8 and Cu2.3-MOR15 are shown in Figure 5(b) and (c), and their structural parameters evaluated by the curve fitting analysis are presented in Table S1. The spectra were well fitted with similar local structure models to Cu2.0-MOR10. Similar spectral change to Cu2.0-MOR10 was observed on Cu2.3-MOR15 observed. Meanwhile, the changes in the second shell peak intensities of Cu2.0-MOR10 and Cu2.3-MOR15 by the reaction gas flow (1) were larger than that of Cu1.1-FAU8. The large changes of the peak intensities of Cu2.0-MOR10 and Cu2.3-MOR15 are accounted for by the large variation of CN(Cu-Al) and CN(Cu-Cu) (Table S1 and Figure S12). The result suggests that the Cu species in MOR has a more dynamic structure or higher mobility in the zeolite framework compared to that in Cu1.1-FAU8. It should also be noted that a similar structural change in Cu2.0-MOR10 by the reaction gas flow to the O_2 pretreated sample is also observed by the wet He flow (Figure 5(d) and Table S1). Thus, H_2O adsorption is responsible for the mobility of the Cu species, which can contribute to the redox cycle, particularly for the oxidation of Cu(I) to Cu(II) with O_2 activation.[31]

The oxidation step has been demonstrated to be the key to the selective catalytic reduction of NOx with NH_3 over Cu zeolite.[31] The rate of oxidation step is controlled by the dynamic multimer formation of Cu(II) species, where O_2 is activated to oxidize Cu(I) when Cu(I) species come across with other one(s) during their diffusion in zeolite channels with the assistance of solvation by NH_3. In the case of the $CH_4/O_2/H_2O$ reaction, H_2O promote diffusion or structural variation of Cu(I) species, as suggested by the change in the FT EXAFS spectra induced by the wet He flow. In addition, such behaviour can stimulate the oxidation of Cu(I) by forming Cu(II) multimers with activated O_2. The diffusion-induced Cu(II) multimer formation is also consistent with a recent study on the catalytic partial oxidation of CH_4 using Cu zeolites.[14] Therefore, one can consider that the catalytic activity of Cu zeolites in the $CH_4/O_2/H_2O$ reaction is affected by formation rate of Cu(II) multimer through diffusion and encountering of two Cu(II) species and O_2. The pore structure of MOR might also contribute to formation of Cu multimer. According to the literature, dinuclear or trinuclear Cu species are formed on the 8 membered ring (8 MR) side pockets of MOR after heat treatment (≥ 450 °C) under dry conditions.[24, 35, 36] It is speculated that the 8 MR side pockets of MOR dynamically interact with hydrated $Cu^{+/2+}$ species under wet conditions of this study, and thus, they can contribute to formation of Cu(II) multimer.

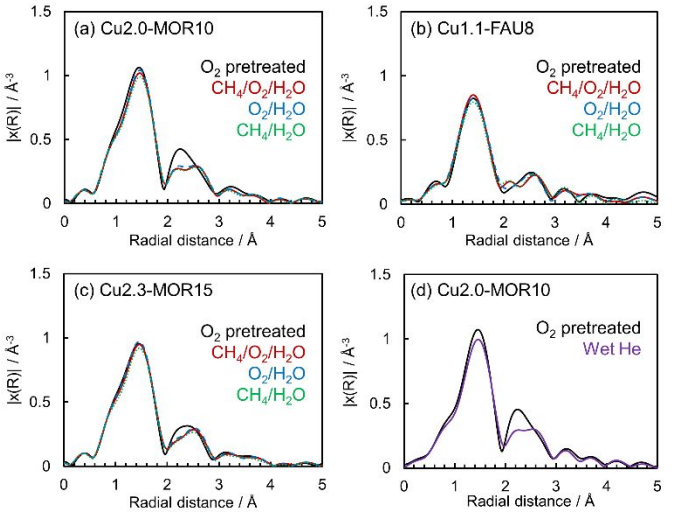

Figure 5. In-situ Cu K-edge FT k^2-weighted EXAFS spectra of (a) Cu2.0-MOR10, (b) Cu1.1-FAU8 and (c) Cu2.3-MOR15 obtained according to Scheme 1: after O_2 pretreatment (black line) and exposure to gas flow conditions (1) (red line), (2) (blue dashed line) and (3) (green dotted line). (d) Cu2.0-MOR10 treated with wet He (purple solid line) after O_2 pretreatment.

Adsorbed intermediates

DRIFT spectra were obtained for Cu2.0-MOR10, Cu1.1-FAU8 and Cu2.3-MOR15 at the same time as the XAFS measurements according to Scheme 1. Figure 6(a)–(c) display the DRIFT spectra in 1400–1700 cm^{-1} region, where many bands mainly due to vibration/rotation of water vapor are observed. The spectra of Cu2.0-MOR10 and Cu2.3-MOR15 exhibit the increase of absorption at 1400-1500 cm^{-1} by flowing the reaction gas (1) (Figure 6(a) and (c)). On the contrary, Cu1.1-FAU8 shows almost no increase at the same region (Figure 6(b)). The increase of IR absorption at 1400-1500 cm^{-1} can be accounted for by formation of methoxy species based on the literature where methoxy species adsorbed on Brønsted acid sites exhibits IR absorption at 1458 cm^{-1}.[37] Accordingly, Cu2.0-MOR10 and Cu2.3-MOR15 form more methoxy species, i.e., the

This journal is © The Royal Society of Chemistry 20xx

Please do not adjust margins

intermediate of CH_3OH, than Cu1.1-FAU8. The result agrees with the difference in the catalytic activity (Figure 1).

In the spectra of Cu2.0-MOR10 and Cu2.3-MOR15, the band intensity at 1400-1500 cm^{-1} is not decreased during the gas flows (2) and (3) (Figure S13 and S14), suggesting relatively strong adsorption of methoxy species on the Brønsted acid sites. One can consider that CH_3OH is not significantly produced through reaction of methoxy on the Brønsted acid sites with H_2O. CH_3OH is considered to be formed through desorption directly from Cu active sites with reaction with H_2O, or through pushing CH_3OH out from the Brønsted acid sites by another CH_3OH supplied from Cu active site.

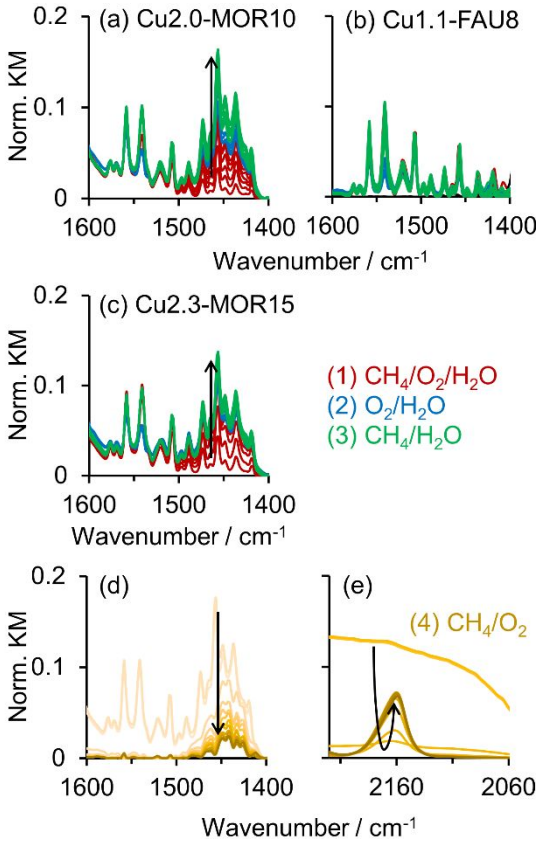

Figure 6. In-situ DRIFT spectra obtained for (a) Cu2.0-MOR10, (b) Cu2.3-MOR15 and (c) Cu1.1-FAU8 under gas flow conditions (1) (red line), (2) (blue line) and (3) (green line) at 1400-1700 cm^{-1} region. DRIFT spectra measured under CH_4/O_2 (dry reaction gas) after (3): (d) 1400-1700 cm^{-1} and (e) 2060-2220 cm^{-1} regions.

When CH_4/O_2 (dry reaction gas) was flown to Cu2.0-MOR10 after the gas flow (3), the IR absorption due to methoxy species is decreased as shown in Figure 6(d). In the meantime, a sharp band appeared at 2158 cm^{-1}, as shown in Figure 6(e), which is assigned to CO adsorbed on Cu(I).[38, 39] It should also be noted that no or very small peak was observed at 2158 cm^{-1} during exposure to (1)–(3) (Figure S13). Thus, CO formed under CH_4/O_2 but not under $CH_4/O_2/H_2O$. This result is consistent with the detected products of the CH_4 oxidation reaction with and without H_2O(g) (Figure 1). Therefore, H_2O(g) is essential for suppressing the overoxidation of CH_4.

Catalytic cycle

Above described XANES spectral analysis with FDMNES simulation has suggested the μ-1,2-peroxo di-Cu (II) and the Cu(I) species with linear coordination geometry as the redox species for CH_4 partial oxidation. In addition, density functional theory (DFT) calculations were conducted to evaluate stability of the μ-1,2-peroxo di-Cu(II) and the bis-μ-oxo di-Cu (II) in a MOR framework where atomic model of MOR zeolite consists of 91 Si atoms, 4 Al atoms and 192 O atoms is used. As a result, the μ-1,2-peroxo-di-Cu (II) is 1.51 eV more stable than the bis-μ-oxo di-Cu (II) within MOR. Thus, the μ-1,2-peroxo-di Cu (II) was proposed to be one of the active structures in the catalytic cycle.

The activation energies for the reduction of the μ-1,2-peroxo-di Cu (II) with CH_4 activation and the oxidation of the Cu(I) species with O_2 activation was evaluated by nudged elastic band calculations. The energy diagrams for both steps are shown in Figure 7. The reduction of the μ-1,2-peroxo di-Cu(II) with CH_4 activation exhibits 0.36 eV of activation energy which is higher than the activation energy of 0.10 eV for the oxidation of the Cu(I). This means that the reduction step is slower than the oxidation step. Diffusion of the Cu(I) species from a MOR cage to neighbouring cage was also evaluated as one can consider that diffusion of Cu(I) spices could be a key for forming the μ-1,2-peroxo di-Cu(II). As shown in Figure 7(c), the activation energy for the diffusion was calculated to be 0.19 eV which is higher than the oxidation step of two Cu(I) species (Figure 7(a)) but smaller than the reduction step of the μ-1,2-peroxo di-Cu(II) species involving C-H activation(Figure 7(b)). Accordingly, the reduction step of the μ-1,2-peroxo di-Cu(II) species with C-H activation has the highest activation energy. Meanwhile, the experimental results indicated that the oxidation of Cu(I) is important for catalytic partial oxidation of CH_4. The contribution of Cu(I) oxidation to the reaction rate is reasonable when the formation rate of the μ-1,2-peroxo di-Cu(II) is kinetically controlled by diffusion and encountering of two Cu(I) species with O_2 activation in the zeolite channel. It should be reminded that Cu2.0-MOR10 and Cu2.3-MOR15 with high catalytic activity have a more dynamic structure or higher mobility of Cu species compared to Cu1.1-FAU8. In addition, the partial oxidation rate of CH_4 was largely improved by increasing O_2 concentration compared to the previous study.[13] Thus, it is reasonable to consider that the kinetics of the formation of Cu(II) multimers affect catalytic partial oxidation of CH_4. If the other Cu multimers such as μ-oxo species concern the catalytic reaction, activation or splitting of O_2 species in Cu multimers can also contribute to the CH_4 oxidation rate. Since the formation rate of active species involving diffusion, encountering and O_2 activation can be increased by increasing reaction temperature, the improved CH_3OH production in this study is also attributable to the higher reaction temperature by 25-50 °C than in the previous studies.[13, 14, 25]

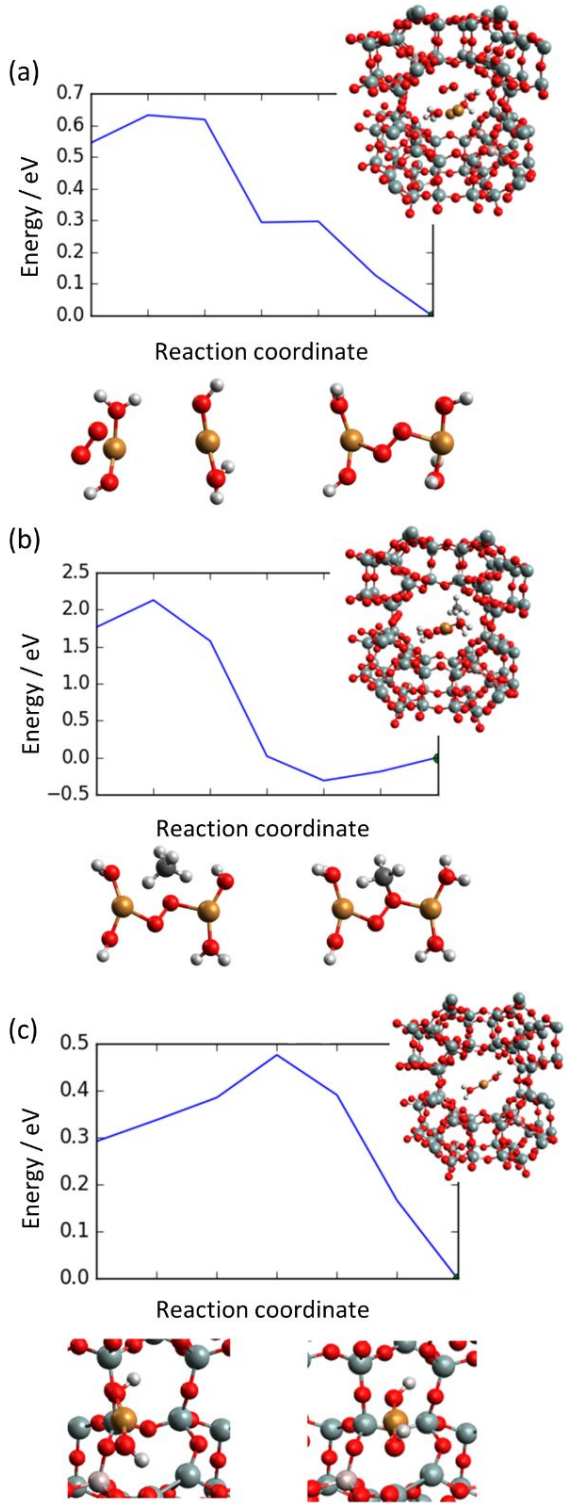

Figure 7. Calculated activation energy diagrams for (a) O_2 activation by two Cu(I) species, (b) CH_4 activation on the μ-1,2-peroxo-di Cu (II) species (c) diffusion of Cu(I) species. Atomic colour code: red: O, white: H, brown: Cu, grey: Si, dark grey: C.

Figure 8 shows the proposed catalytic cycle of the Cu-MOR in the $CH_4/O_2/H_2O$ reaction. Under the humidified atmosphere, the μ-1,2-peroxo di-Cu (II) react with CH_4 to form CH_3OH and Cu(I) species, which is oxidized by encountering another Cu(I) and O_2 to regenerate the μ-1,2-peroxo di-Cu (II). The diffusion involved oxidation step of Cu(I) to Cu(II) species can be the key step in this catalytic cycle over Cu species in zeolites.

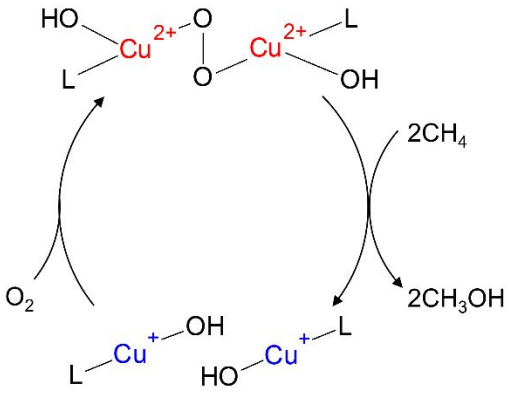

Figure 8. Proposed catalytic cycle for the $CH_4/O_2/H_2O$ reaction over Cu zeolites. L is H_2O or oxygen of the zeolite framework.

Conclusions

Cu zeolites behave as catalysts for the direct oxidation of CH_4 to CH_3OH under $CH_4/O_2/H_2O$ flow conditions. Among the various Cu zeolites tested, the Cu-MOR catalysts showed relatively high CH_3OH production, with Cu2.0-MOR10 achieving a TON of 7.4 mol_{CH3OH}/mol_{Cu} over 24 h (CH_4 conv.: 0.011%). The total TON of CH_3OH and HCHO production was 10.9 $mol_{CH3OH+HCHO}/mol_{Cu}$. In-situ simultaneous XAFS and DRIFT spectral analyses unveiled the catalytic cycle, in which Cu (II) multimers react with CH_4 to form the linearly coordinated Cu(I) species and CH_3OH, and then the Cu(I) species is oxidized by O_2 to close the catalytic cycle. The main feature of the catalytic cycle is the redox reactions of Cu(I)/Cu(II) species. In particular, the oxidation of Cu(I) to Cu (II) was observed on Cu2.0-MOR10 and Cu2.3-MOR15 showing relatively high catalytic activity, but barely on Cu1.1-FAU8 showing low catalytic activity. In addition, the Cu-MOR catalysts showed dynamic structure of Cu species with H_2O adsorption. Therefore, the Cu species having high mobility by H_2O adsorption is crucial for oxidation of the Cu(I) species, and for CH_3OH production in the $CH_4/O_2/H_2O$ reaction. The results of this study reveal new catalyst and process designs to further improve our capability for direct oxidation of CH_4 to CH_3OH.

Methods

Catalyst preparation

MOR10, MOR15, MOR110, BEA20, FAU8, MFI12 and MFI19 zeolites are 640HOA, 660HOA, 690HOA, 940HOA, 360HUA, 822HOA and 840HOA supplied from Tosoh, respectively. The Cu-exchanged zeolites were prepared by an ion exchange method. Each zeolite (2 g) was added to an aqueous solution of $Cu(CH_3COO)_2 \cdot H_2O$ (200 mL). After stirring at 80 °C for 3 h, the suspension was filtered. The residue was washed with water,

This journal is © The Royal Society of Chemistry 20xx

Please do not adjust margins

dried at 110 °C overnight and calcined at 700 °C for 1 h to obtain each Cu zeolite.

Catalytic test

The $CH_4/O_2/H_2O$ reaction was performed using a fixed-bed flow reactor with catalyst (50 mg) inside a quartz glass tube with an inner diameter of 4 mm (Figure S15). The catalyst was pretreated under O_2 flow (15 mL min^{-1}) at 550 °C for 30 min. After the catalyst was cooled to 300 °C and purged with N_2 (50 mL min^{-1}) for 30 min, the reaction gas composed of CH_4 (48 mL min^{-1}) + O_2 (2 mL min^{-1}) + N_2 (50 mL min^{-1}) + H_2O(g) (0.5 g h^{-1}) was fed into the catalyst bed. H_2O(g) was supplied using a controlled evaporation and mixing system (Bronkhorst μ-FLOW L01 and CEM W-101A). The outlet gas was analysed by GC (Shimadzu GC-2014) with a methanizer equipped with an FID and TCD. The outlet gas was trapped at ca. 10 °C. The trapped liquid was analysed using a HPLC system (JASCO) with a Shodex RSpak DE-413L column (Showa Denko). The yield of CH_3OH was calculated by integrating CH_3OH gas concentration analysed by the GC-FID. The yields of CH_3OH was also determined by the HCPL analysis of the trapped liquids with correction of evaporated amount based on Raoult's law where 5692 Pa (9.96 °C) was used as CH_3OH vapor pressure. In the case of HCHO concentration, most of HCHO is assumed to be hydrated to methanediol ($H_2C(OH)_2$), and evaporated amount of HCHO is assumed to be very small (< 0.4% of total HCHO amount based on estimation using 16.1 Pa (25 °C) of $H_2C(OH)_2$ vapor pressure) enough to be ignored.

Characterisation

Cu loading was determined by inductively coupled plasma-optical emission spectroscopy (ICP-OES, Thermo iCAP7400) and X-ray fluorescence (Rigaku EDXL 300). Samples for ICP-OES were prepared by a fusion method.[40] Cu zeolite (20 mg) was mixed with sodium peroxide (0.5 g) in a zirconium crucible and then the mixture was heated at 500 °C. The molten samples were dissolved by addition of 2 M HCl (20 mL).

In-situ XAFS and DRIFTS measurements were performed on BL01B1 at SPring-8. A schematic diagram of the optical system is presented in Figure S16. A sample pellet with a diameter of 7 mm was set in an in-situ cell with two Kapton windows on the top and bottom of the pellet for XAFS measurements and two CaF_2 windows at 30° to one side of the pellet for DRIFTS measurements. The in-situ cell was also equipped with a heater, gas inlet and gas outlet to allow gas flow through the sample pellet at given temperatures. The gas flow and temperature were changed according to Scheme 1, S1, and S2. H_2O(g) was supplied using a water bubbler at 50 °C. XAFS spectra were collected at 10-min intervals in a quick scan mode by a transmission method using ion chambers. DRIFT spectra were obtained on a Bruker Vertex70 with a mercury/cadmium/telluride detector. A DRIFT background spectrum was measured under the He flow after pretreatment and the sample spectra were collected at 10-min intervals under the various gas flow conditions. DRIFT spectra were normalised by the intensity of the band related to the vibration/rotation of CH_4, which was determined by subtracting the intensity at 2937 cm^{-1} at the end of gas flow conditions (2) from that of (1) (Figure S13). XAFS data were analysed using the Athena software included in the Demeter package.

XANES simulation

XANES simulation is performed by FDMNES II program (Revision 18th) under the condition of full multiple scattering mode with 6A radius in non-periodic state.[30] The structures of active Cu species within ground state (See Figure 3 (b)) are applied as calculation models.

First Principle calculation Method and Model

First principle calculations are carried out in order to understand the Cu oxidation and methane activation. In particular, grid based projector augmented wave (GPAW) method within density functional theory is implemented.[41] Exchange-correlation of PBE is applied for all calculations.[42] 2x2x2 special k points of the Brillouin zone sampling are used where periodic boundary condition is applied for all direction.[43] Nudged elastic band method is implemented for transition state calculations.[44]

Author Contributions

J.O. conceived the idea, designed the experiments, analysed the data and wrote the manuscript. A.H. conducted the experiments, analysed the data and wrote the manuscript. Y.T. contributed the in-situ analysis. N.K. prepared the catalysts. S.N. contributed to the catalyst preparation, reaction evaluation, and XAFS-DRIFT measurements. K.K. contributed to the XAFS-DRIFT measurements and data analysis. Y.H. and M.M. participated in the reaction evaluation. I.M. and K.T. performed the XANES simulation and DFT calculations. All authors discussed the results and commented on the manuscript.

Conflicts of interest

There are no conflicts to declare.

Acknowledgements

This work was funded in part by the Japan Science and Technology Agency (JST) CREST (JPMJCR17P2) and the Japan Society for the Promotion of Science (JSPS) KAKENHI through a Grant-in-Aid for Scientific Research (B) (20H02524). The in situ XAFS-DRIFT spectral measurements were conducted on BL01B1 at SPring-8 (Proposal Nos. 2017B1958, 2018A2070, 2018B2110, 2019A2066, 2019B1188). We thank Natasha Lundin, PhD, from Edanz Group (https://en-author-services.edanzgroup.com/) for editing a draft of this manuscript.

References

1 V. L. Sushkevich, D. Palagin, M. Ranocchiari and J. A. van Bokhoven, *Science*, 2017, **356**, 523-527.

2 E. V. Kondratenko, T. Peppel, D. Seeburg, V. A. Kondratenko, N. Kalevaru, A. Martin and S. Wohlrab, *Catal. Sci. Tech.*, 2017, **7**, 366-381.

3 E. G. Nisbet, E. J. Dlugokencky and P. Bousquet, *Science*, 2014, **343**, 493-495.
4 M. H. Mahyuddin, Y. Shiota and K. Yoshizawa, *Catal. Sci. Tech.*, 2019, **9**, 1744-1768.
5 Z. Liang, T. Li, M. Kim, A. Asthagiri and J. F. Weaver, *Science*, 2017, **356**, 299-303.
6 J.-P. Lange, V. L. Sushkevich, A. J. Knorpp and J. A. van Bokhoven, *Ind. Eng. Chem. Res*, 2019, **58**, 8674-8680.
7 K. Murata, Y. Mahara, J. Ohyama, Y. Yamamoto, S. Arai and A. Satsuma, *Angew. Chem. Int. Ed.*, 2017, **56**, 15993-15997.
8 M. Cargnello, J. J. D. Jaen, J. C. H. Garrido, K. Bakhmutsky, T. Montini, J. J. C. Gamez, R. J. Gorte and P. Fornasiero, *Science*, 2012, **337**, 713-717.
9 S. Sirajuddin and A. C. Rosenzweig, *Biochemistry*, 2015, **54**, 2283-2294.
10 B. E. R. Snyder, M. L. Bols, R. A. Schoonheydt, B. F. Sels and E. I. Solomon, *Chem. Rev.*, 2018, **118**, 2718-2768.
11 A. R. Kulkarni, Z.-J. Zhao, S. Siahrostami, J. K. Nørskov and F. Studt, *Catal. Sci. Tech.*, 2018, **8**, 114-123.
12 M. Ravi, M. Ranocchiari and J. A. van Bokhoven, *Angew. Chem. Int. Ed.*, 2017, **56**, 16464-16483.
13 K. Narsimhan, K. Iyoki, K. Dinh and Y. Román-Leshkov, *ACS Cent. Sci.*, 2016, **2**, 424-429.
14 K. T. Dinh, M. M. Sullivan, K. Narsimhan, P. Serna, R. J. Meyer, M. Dincă and Y. Román-Leshkov, *J. Am. Chem. Soc.*, 2019, **141**, 11641-11650.
15 T. Sheppard, C. D. Hamill, A. Goguet, D. W. Rooney and J. M. Thompson, *Chem. Commun.*, 2014, **50**, 11053-11055.
16 M. V. Parfenov, E. V. Starokon, L. V. Pirutko and G. I. Panov, *J. Catal.*, 2014, **318**, 14-21.
17 C. Hammond, M. M. Forde, M. H. Ab Rahim, A. Thetford, Q. He, R. L. Jenkins, N. Dimitratos, J. A. Lopez-Sanchez, N. F. Dummer, D. M. Murphy, A. F. Carley, S. H. Taylor, D. J. Willock, E. E. Stangland, J. Kang, H. Hagen, C. J. Kiely and G. J. Hutchings, *Angew. Chem. Int. Ed.*, 2012, **51**, 5129-5133.
18 P. Xiao, Y. Wang, T. Nishitoba, J. N. Kondo and T. Yokoi, *Chem. Commun.*, 2019, **55**, 2896-2899.
19 C. Hammond, N. Dimitratos, R. L. Jenkins, J. A. Lopez-Sanchez, S. A. Kondrat, M. Hasbi ab Rahim, M. M. Forde, A. Thetford, S. H. Taylor, H. Hagen, E. E. Stangland, J. H. Kang, J. M. Moulijn, D. J. Willock and G. J. Hutchings, *ACS Catal.*, 2013, **3**, 689-699.
20 C. Hammond, R. L. Jenkins, N. Dimitratos, J. A. Lopez-Sanchez, M. H. ab Rahim, M. M. Forde, A. Thetford, D. M. Murphy, H. Hagen, E. E. Stangland, J. M. Moulijn, S. H. Taylor, D. J. Willock and G. J. Hutchings, *Chem. Euro. J.*, 2012, **18**, 15735-15745.
21 M. H. Groothaert, P. J. Smeets, B. F. Sels, P. A. Jacobs and R. A. Schoonheydt, *J. Am. Chem. Soc.*, 2005, **127**, 1394-1395.
22 P. Tomkins, A. Mansouri, S. E. Bozbag, F. Krumeich, M. B. Park, E. M. C. Alayon, M. Ranocchiari and J. A. van Bokhoven, *Angew. Chem. Int. Ed.*, 2016, **128**, 5557-5561.
23 D. K. Pappas, E. Borfecchia, M. Dyballa, I. A. Pankin, K. A. Lomachenko, A. Martini, M. Signorile, S. Teketel, B. Arstad, G. Berlier, C. Lamberti, S. Bordiga, U. Olsbye, K. P. Lillerud, S. Svelle and P. Beato, *J. Am. Chem. Soc.*, 2017, **139**, 14961-14975.
24 G. Brezicki, J. D. Kammert, T. B. Gunnoe, C. Paolucci and R. J. Davis, *ACS Catal.*, 2019, **9**, 5308-5319.
25 A. Koishybay and D. F. Shantz, *J. Am. Chem. Soc.*, 2020, **142**, 11962-11966.
26 A. Martini, E. Borfecchia, K. A. Lomachenko, I. A. Pankin, C. Negri, G. Berlier, P. Beato, H. Falsig, S. Bordiga and C. Lamberti, *Chem. Sci.*, 2017, **8**, 6836-6851.
27 R. A. Bair and W. A. Goddard, *Phis. Rev. B*, 1980, **22**, 2767-2776.
28 N. Kosugi, T. Yokoyama, K. Asakura and H. Kuroda, *Chem. Phys.*, 1984, **91**, 249-256.
29 L. S. Kau, D. J. Spira-Solomon, J. E. Penner-Hahn, K. O. Hodgson and E. I. Solomon, *J. Am. Chem. Soc.*, 1987, **109**, 6433-6442.
30 Y. Joly, *Phis. Rev. B*, 2001, **63**, 125120.
31 C. Paolucci, I. Khurana, A. A. Parekh, S. C. Li, A. J. Shih, H. Li, J. R. Di Iorio, J. D. Albarracin-Caballero, A. Yezerets, J. T. Miller, W. N. Delgass, F. H. Ribeiro, W. F. Schneider and R. Gounder, *Science*, 2017, **357**, 898-903.
32 R. Cao, C. Saracini, J. W. Ginsbach, M. T. Kieber-Emmons, M. A. Siegler, E. I. Solomon, S. Fukuzumi and K. D. Karlin, *J. Am. Chem. Soc.*, 2016, **138**, 7055-7066.
33 S. Grundner, M. A. C. Markovits, G. Li, M. Tromp, E. A. Pidko, E. J. M. Hensen, A. Jentys, M. Sanchez-Sanchez and J. A. Lercher, *Nat. Commun.*, 2015, **6**, 7546.
34 V. L. Sushkevich, O. V. Safonova, D. Palagin, M. A. Newton and J. A. van Bokhoven, *Chem. Sci.*, 2020, **11**, 5299-5312.
35 S. Grundner, W. Luo, M. Sanchez-Sanchez and J. A. Lercher, *Chem. Commun.*, 2016, **52**, 2553-2556.
36 P. Vanelderen, B. E. R. Snyder, M.-L. Tsai, R. G. Hadt, J. Vancauwenbergh, O. Coussens, R. A. Schoonheydt, B. F. Sels and E. I. Solomon, *J. Am. Chem. Soc.*, 2015, **137**, 6383-6392.
37 V. L. Sushkevich, R. Verel and J. A. van Bokhoven, *Angew. Chem. Int. Ed.*, 2020, **59**, 910-918.
38 K. Hadjiivanov, D. Klissurski, G. Ramis and G. Busca, *Appl. Catal. B*, 1996, **7**, 251-267.
39 T. Pieplu, F. Poignant, A. Vallet, J. Saussey, J. C. Lavalley and J. Mabilon, in *Stud. Surf. Sci. Catal.*, eds. A. Frennet and J. M. Bastin, Elsevier, 1995, vol. 96, pp. 619-629.
40 T. Sheppard, H. Daly, A. Goguet and J. M. Thompson, *ChemCatChem*, 2016, **8**, 562-570.
41 J. J. Mortensen, L. B. Hansen and K. W. Jacobsen, *Phis. Rev. B*, 2005, **71**, 035109.
42 J. P. Perdew, K. Burke and M. Ernzerhof, *Phys. Rev. Lett.*, 1996, **77**, 3865-3868.
43 H. J. Monkhorst and J. D. Pack, *Phis. Rev. B*, 1976, **13**, 5188-5192.
44 G. Henkelman, B. P. Uberuaga and H. Jónsson, *J. Chem. Phys.*, 2000, **113**, 9901-9904.

This journal is © The Royal Society of Chemistry 20xx

Please do not adjust margins